Monthly Notices of the ROYAL ASTRONOMICAL SOCIETY

MNRAS **540,** 3281–3288 (2025) https://doi.org/10.1093/mnras/staf857
Advance Access publication 2025 June 4

Lopsidedness in early-type galaxies: the role of the $m = 1$ multipole in isophote fitting and strong lens modelling

A. Amvrosiadis,[1]★ J. W. Nightingale [1,2,3] Q. He [1] A. Robertson [4] S. Lange [1] C. S. Frenk,[1] S. Cole,[1] R. Massey [1,2] and A. Poci [5]

[1]*Department of Physics, Institute for Computational Cosmology, Durham University, South Road, Durham DH1 3LE, UK*
[2]*Department of Physics, Centre for Extragalactic Astronomy, Durham University, South Road, Durham DH1 3LE, UK*
[3]*School of Mathematics, Statistics and Physics, Newcastle University, Newcastle upon Tyne NE1 7RU, UK*
[4]*Carnegie Observatories, 813 Santa Barbara Street, Pasadena, CA 91101, USA*
[5]*Sub-department of Astrophysics, Department of Physics, University of Oxford, Denys Wilkinson Building, Keble Road, Oxford OX1 3RH, UK*

Accepted 2025 April 30. Received 2025 April 7; in original form 2024 July 2

ABSTRACT

The surface brightness distribution of massive early-type galaxies (ETGs) often deviates from a perfectly elliptical shape. To capture these deviations in their isophotes during an ellipse fitting analysis, Fourier modes of order $m = 3, 4$ are often used. In such analyses, the centre of each ellipse is treated as a free parameter which may result in offsets from the centre of light, particularly for ellipses in the outer regions. This complexity is not currently accounted for in the mass models used in either strong gravitational lensing or galactic dynamical studies. In this work, we adopt a different approach, using the $m = 1$ Fourier mode to account for this complexity while keeping the centres of all perturbed ellipses fixed, showing that it fits the data equally well. We applied our method to the distribution of light emission to a sample of ETGs from the MASSIVE survey and found that the majority have low m_1 amplitudes, below 2 per cent. Five out of the 30 galaxies we analysed have high m_1 amplitudes, ranging from 2 to 10 per cent in the outer parts ($R \gtrsim 3$ kpc), all of which have a physically associated companion. Based on our findings, we advocate the use of the $m = 1$ multipole in the mass models used in strong lensing and dynamical studies, particularly for galaxies with recent or ongoing interactions.

Key words: gravitational lensing: strong – galaxies: elliptical and lenticular – galaxies: structure.

1 INTRODUCTION

The most massive early-type galaxies (ETGs) in the local Universe emerged from high-density regions of the primordial matter distribution (Blumenthal et al. 1984; Frenk et al. 1985). Galaxy interactions and mergers, which are expected to be frequent in dense environments, affect their morphologies and kinematics.

ETGs are approximately elliptical in shape and are typically modelled as such. However, a large fraction of ETGs have surface brightness profiles that exhibit deviations from perfect ellipses. These deviations are evident in the isophotes, which can take on boxy or discy shapes (Bender & Moellenhoff 1987; Bender, Doebereiner & Moellenhoff 1988; Bender et al. 1989; Hao et al. 2006; Chaware et al. 2014; Goullaud et al. 2018), as well as in variations of the position angle of their isophotes as a function of radius, known as isophotal twists (Cappellari 2002). These azimuthal asymmetries likely reflect the complex gravitational dynamics at play during the formation and evolution of the galaxy and it is unsurprising that they often exhibit radial trends.

One approach to parametrize these deviations is through the use of high-order Fourier modes (i.e. multipoles; see Section 3), typically of order $m = 3, 4$ (e.g. Hao et al. 2006; Goullaud et al. 2018; see also multigaussian expanion). For instance, the $m = 4$ multipole can account for boxiness or disciness in the light distribution (e.g. Bender & Moellenhoff 1987; Bender et al. 1988, 1989). The typical amplitudes of these multipoles are found to be up to ∼1 per cent (e.g. Hao et al. 2006; Pasquali et al. 2006; Goullaud et al. 2018). It is important to note that studies employing an ellipse fitting technique to analyse the isophotes of ETGs allow the centres of the ellipses to vary. In a few cases, fractional offsets, $\Delta R/R$, are found, which can be as large as 10–15 per cent at $R > 5$ kpc (Fig. 3 in Goullaud et al. 2018). We will refer to this later type of complexity as lopsidedness.

The types of complexity discussed above are also expected to be present in the mass distribution of galaxies. Strong gravitational lensing is a powerful tool for constraining the mass distribution of galaxies acting as lenses. Utilizing strong lensing, many recent studies have shown that angular complexity in the mass distribution, in the form of $m = 3, 4$ multipoles, is strongly favoured by the data (e.g. Hezaveh et al. 2016; Powell et al. 2022; Van de Vyvere et al. 2022; Ballard et al. 2024; Cohen et al. 2024; Nightingale et al. 2024; Stacey et al. 2024), with the level of correction matching those found from ellipse fitting to the light distribution (∼1–2 per cent). However, commonly used mass models in strong lensing lack the flexibility to account for features such as lopsidedness (isodensity contours are assumed to share a common centre), and therefore some of these

★ E-mail: aristeidis.amvrosiadis@durham.ac.uk

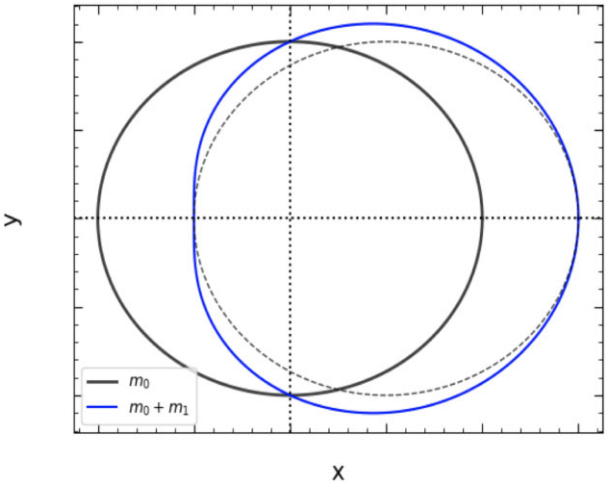

Figure 1. Example of how a circular path, m_0 (black; solid), is perturbed by an $m = 1$ multipole (blue; solid), where the position angle, ϕ_1, of the m_1 mode is aligned with the x-axis. For comparison, we show a circular path that has been shifted in the x-axis (black; dashed) by the same amount as the m_1 amplitude.

measurements could be biased. The lens models used in Nightingale et al. (2019, 2023) favoured stellar mass profiles with centre offsets of order 100–300 pc, which the authors suggested is evidence for lopsidedness in the mass distribution.

In this work, we propose the use of the $m = 1$ multipole to account for lopsidedness in the light/mass distribution of ETGs. Our objective is to showcase the utility of the $m = 1$ multipole in ellipse fitting analyses as an alternative to allowing the centres of ellipses to vary (the former can be easily implemented in mass models used for strong gravitational lensing). To achieve this, we conduct an isophotal analysis of a sample of the most massive ETGs in the local Universe from the MASSIVE survey. It is important to note that an $m = 1$ Fourier mode is not equivalent to a positional shift of the ellipse's centre (as demonstrated in Fig. 1). We expect these to not be fully independent, especially in strong lensing studies (Lange et al. 2025; Amvrosiadis et al. in preparation).

The outline of the paper is as follows. In Section 2, we introduce the sample used in this work. In Section 3, we describe our method to extract isophotal fit parameters. In Section 4, we present our results. Finally, in Section 5, we discuss these results and place them in the context of strong lensing and galactic dynamics. Finally, in Section 6, we present our conclusions. Throughout this work, we adopt a spatially flat Lambda cold dark matter cosmology with $H_0 = 67.8 \pm 0.9\,\mathrm{km\,s^{-1}\,Mpc^{-1}}$ and $\Omega_\mathrm{M} = 0.308 \pm 0.012$ (Planck Collaboration XIII 2016).

2 OBSERVATIONS

The sample we adopt was first introduced in Goullaud et al. (2018), which is comprised of 35 galaxies selected from the MASSIVE survey (Ma et al. 2014), a volume-limited ($D < 108$ Mpc) survey of 116 ETGs. The galaxies in this sample were observed with the *Hubble Space Telescope* (*HST*), for one orbit, in the F110W filter with exposure times between 2500 and 2900 sec.

We excluded a few sources in our analysis from the original sample of Goullaud et al. (2018): NGC0545, NGC0547, NGC1684, NGC5353, and NGC6482. These exclusions were due to our inability to obtain a good fit to their isophotes. However, it is important to note that the primary aim of this work is to demonstrate the effectiveness of the m_1 multipole compared to a variable ellipse centre for isophotal analysis (as discussed later in Section 4). Therefore, removing sources that are challenging to fit, regardless of whether using an m_1 or variable centre, does not diminish the validity of our overall conclusions.

3 ISOPHOTE FITTING

We developed our own routine to perform the ellipse fitting analysis which simultaneously optimizes the parameters of the ellipse ($\boldsymbol{\theta}_\mathrm{e}$: x_0, y_0, e, θ), and the parameters of the multipole perturbations ($\boldsymbol{\theta}_\mathrm{m}$: a_m, b_m for $m = 1, 3, 4$) and builds on previous methods (e.g. Bender & Moellenhoff 1987; Hao et al. 2006; Goullaud et al. 2018).

The equation of an ellipse in polar coordinates, $r_\mathrm{e}(\phi)$, is given by

$$r_\mathrm{e}(\phi) = \frac{a(1-e^2)}{\sqrt{1 + e\cos(\phi - \theta)}}\,, \tag{1}$$

where a is the major axis, e is the ellipticity, and θ is the position angle of the major axis. We add perturbations to that ellipse in the form of multipoles given by,

$$r_\mathrm{m}(\phi) = a_\mathrm{m}\cos\left[m\,(\phi - \theta)\right] + b_\mathrm{m}\sin\left[m\,(\phi - \theta)\right]\,, \tag{2}$$

where m is the harmonic mode. We only consider multipoles of order $m = 1, 3, 4$ as the $m = 2$ is already included in the model (i.e. ellipticity).

From the above equations, the perturbed elliptical path in polar coordinates is given by, $r(\phi) = r_\mathrm{e}(\phi) + r_\mathrm{m}(\phi)$. In a Cartesian system, the (x, y) coordinates of the perturbed elliptical path can then be computed as,

$$x = x_0 + r(\phi)\cos\phi$$
$$y = y_0 + r(\phi)\sin\phi,$$

where (x_0, y_0) correspond to the centre of the ellipse.

We optimize the parameters of the perturbed ellipse for different fixed values of the major axis, a, which are logarithmically spaced. During optimization we aim to maximize the log of the likelihood function given by

$$L = -\sum_{\phi=0}^{360}\left(\frac{\mathrm{I}(\phi|\boldsymbol{\theta}_\mathrm{e}, \boldsymbol{\theta}_\mathrm{m}) - \langle\mathrm{I}(\phi|\boldsymbol{\theta}_\mathrm{e}, \boldsymbol{\theta}_\mathrm{m})\rangle}{\sigma_\mathrm{I}}\right)^2, \tag{3}$$

where $\mathrm{I}(\phi|\boldsymbol{\theta}_\mathrm{e}, \boldsymbol{\theta}_\mathrm{m})$ is the intensity profile along the perturbed elliptical path constructed from the $(\boldsymbol{\theta}_\mathrm{e}, \boldsymbol{\theta}_\mathrm{m})$ set of parameters.[1] with $\langle\mathrm{I}\rangle$ representing the median of these values[2] and σ_I is the error map (we use the WHT map of the *HST* data products).

The parameter optimization is carried out using the EMCEE package (Foreman-Mackey et al. 2013) for each of the isophotes independently. The centre of the perturbed ellipses is kept fixed during optimization to the value we estimate for the innermost ellipse. A few galaxies in this sample have dust lanes in their central regions, which can prevent an accurate centre determination. In these cases the innermost ellipse is shifted outwards.

[1]The observed images are first interpolated on a regular grid so that we can sample the intensity at any (x, y) location.

[2]Subtracting the mean of values along the path reduces the number of parameters, we fit for and is equivalent to requiring that the intensity is constant along the path (the definition of an isophote). Alternatively, one can introduce an additional parameter for the intensity as it is typically done.

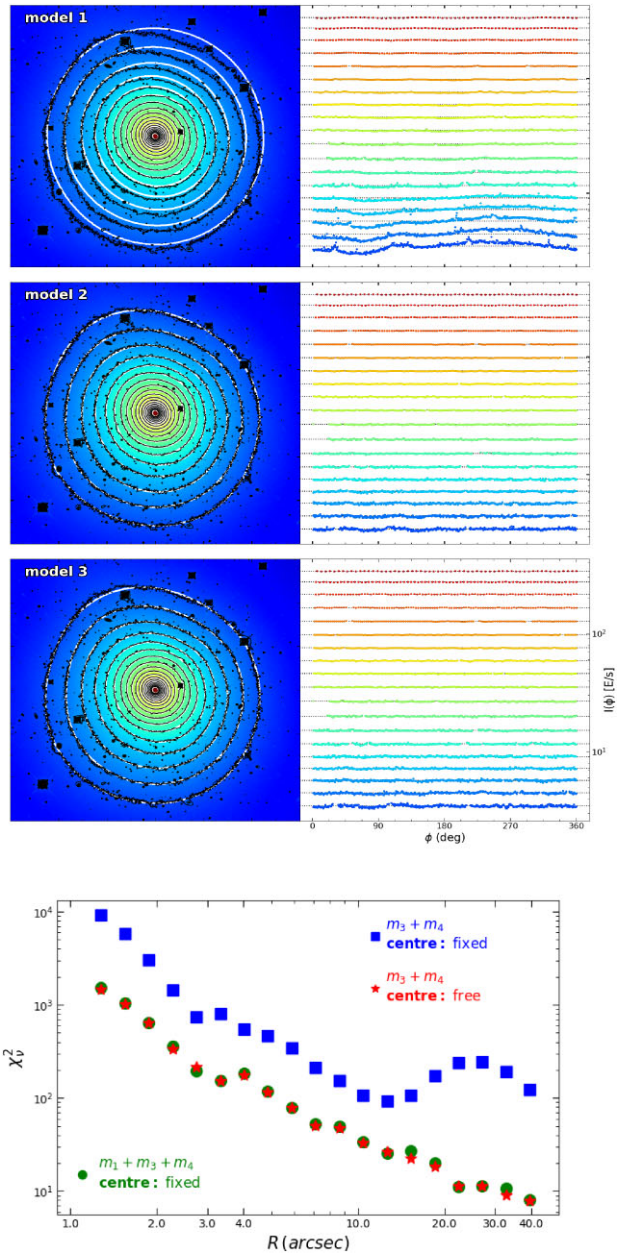

Figure 2. Example of our ellipse fitting method applied to NGC2274. The panels from top to bottom correspond to models: (i) multipoles: $m = 3, 4$; centre: fixed, (ii) multipoles: $m = 3, 4$; centre: free, and (iii) multipoles: $m = 1, 3, 4$; centre: fixed. The bottom panel show the reduced chi-square of isophotes for the above three models, as a function of galactocentric radius (see also Appendix A2).

4 RESULTS

In Fig. 2, we show an example of our isophotal analysis applied to NGC2274. We examine three cases: **(model 1)** $m = 3,\ 4$ and fixed centre, **(model 2)** $m = 3,\ 4$ and free centre, **(model 3)** $m = 1,\ 3,\ 4$ and fixed centre. For model 1, the extracted isophotal intensity profile notably deviates from a flat trend, particularly evident for the outermost ellipses ($R > 10$ arcsec; approximately 3 kpc at $z = 0.015$; right-hand panel in the top figure), indicating a clear first-order perturbation in the extracted isophotes. In contrast, in model 2 where we allow the centre to vary freely, the fit improves significantly. We observe an increasing fractional offset for ellipses ($\Delta R/R$) as distance from the galactic centre increases, consistent with findings in Goullaud et al. (2018). Finally, both model 2 and 3 provide equally satisfactory fits to the data, assessed using the reduced chi-square as the figure of merit, as illustrated in the bottom panel of Fig. 2. This suggests that the $m = 1$ parametrization can effectively describe the light (or mass) distribution of ETGs without necessitating a variable centre. Moreover, this parametrization offers a straightforward application for mass models used in strong lensing and galaxy dynamics, which can be physically interpreted as lopsidedness (or skewness).

In Fig. 3, we present the radial profiles of m_1 amplitudes extracted from our isophotal analysis for all the galaxies we analysed. The overall shape of the m_1 amplitude profiles displays similar features to the fractional offset profiles in Goullaud et al. (2018). The peak m_1 amplitude we measure is ∼10 per cent, which is slightly lower compared to the maximum fractional offset, $\max\{\Delta R/R\}$ ∼15 per cent, in Goullaud et al. (2018).

Most profiles show a decline in the inner regions, extending out to $R \sim 5$ arcsec, while the remainder remain flat. This inner decline in m_1 amplitude is consistent with the trends observed in Goullaud et al. (2018), where isophotal ellipses exhibit a variable centre. The authors attribute this effect to the presence of dust, which can introduce apparent shifts in the isophotal centre. We note, however, that such dust-induced variations should not impact lensing or dynamical models (see Section 5).

Beyond $R > 5$ arcsec, the m_1 profiles remain flat, for most galaxies, with amplitudes below 2 per cent. Among the 30 sources analysed, only five display a gradual increase in m_1 amplitude with radius, peaking around 20–30 arcsec (∼ 6−10 kpc for $z = 0.015$). In the following section, we discuss the origin for the high m_1 amplitudes in these galaxies.

In Fig. A1, we show the radial profiles for the $m = 3$ and $m = 4$ multipoles, and note that these are consistent with those in Goullaud et al. (2018). Therefore, irrespective of how we parametrize the isophotal path (i.e. either as a radial offset or an $m = 1$ multipole), higher order multipole measurements remain unchanged.

5 DISCUSSION

In this section, we discuss the possible physical origin of an $m = 1$ multipole and the possible consequences of not including this type of complexity in mass models used in strong gravitational lensing and galaxy dynamics.

5.1 The origin of an $m = 1$ multipole

In the top panels of Fig. 3, we show cut-outs of some of the galaxies in our sample. The top row shows galaxies with companions and low m_1 amplitudes (<2 per cent), while the bottom row shows all galaxies with high m_1 amplitudes. These all have a physically associated companion ∼10−40 kpc away from their galactic centre in projection. This suggests that high m_1 amplitudes (or ellipse offsets) are the result of tidal interactions, where the outermost stellar orbits are highly eccentric (Goullaud et al. 2018). Using K-band magnitudes, M_K, we estimate the stellar mass ratios (between the main galaxy and its companion), for those with high m_1 amplitudes, to lie in the range ∼10–250 (see Table 1).

We also tested whether we are artificially measuring high m_1 amplitudes due to light contamination from the companion galaxies. To conduct this test, we created a simulated observation of a physically unassociated galaxy pair (i.e. superposition of two galaxies). We used a Sérsic profile (Sérsic 1963) for the surface brightness distribution

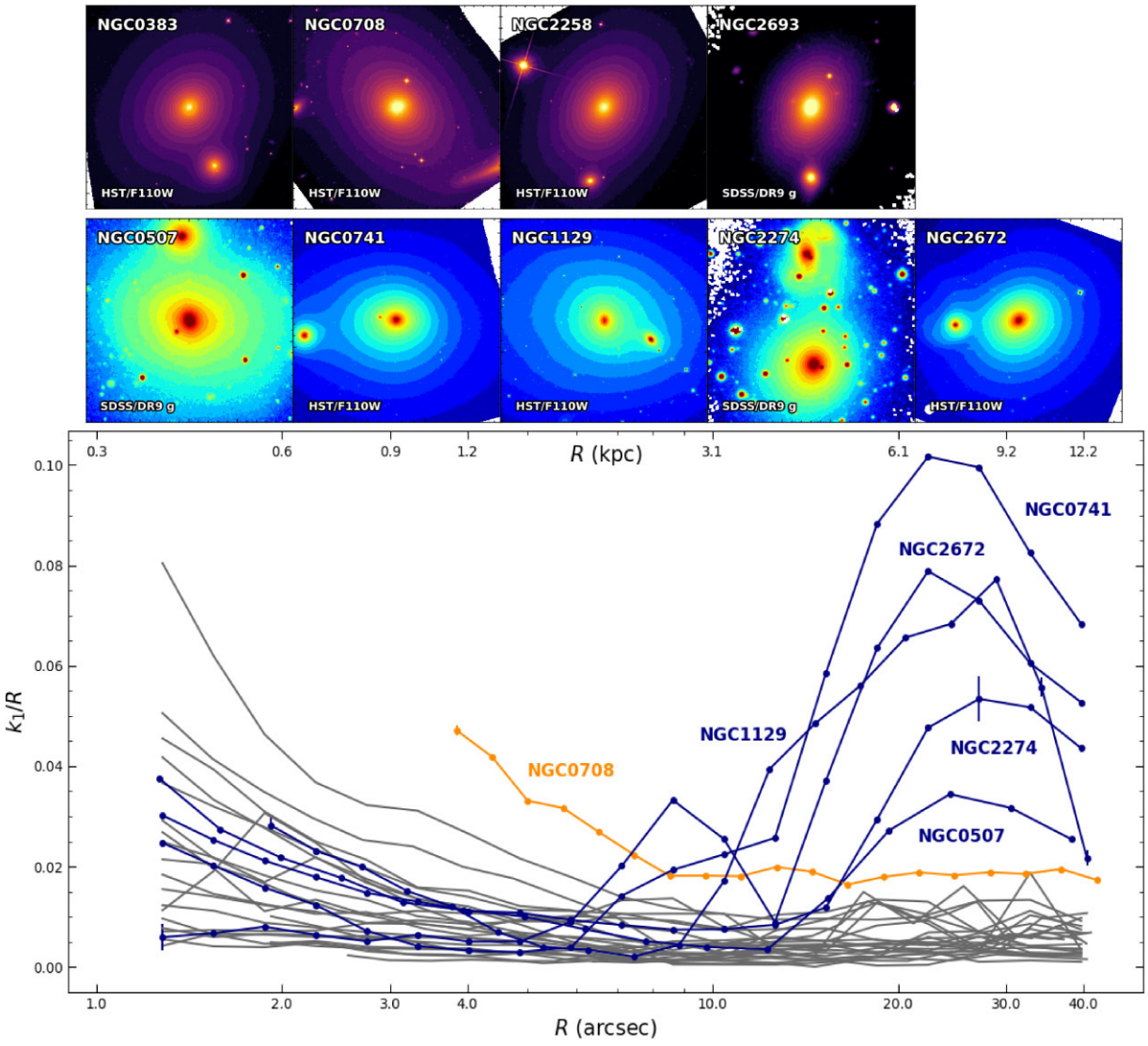

Figure 3. The m_1 amplitude radial profiles for all sources in our sample. We show in blue galaxies with a visible companion galaxy, encompassing all those with high (>2 per cent) m_1 amplitudes. NGC0708, shown in orange, has the most pronounced dust lanes. The top row cutouts show galaxies with companions and low m_1 amplitude, while the second row show galaxies with high m_1 amplitudes. For some of these galaxies the field of view of *HST* is too small to see the companion (e.g. NGC 2274). In these cases, we show a *g*-band image taken from the legacy surveys. North in up in all images.

Table 1. (1) Name; (2) spectroscopic redshift; (3) *K*-band absolute magnitude computed as, $M_K = K - 5\log_{10} D - 25$, where K is taken from the 2MASS catalogue ('k_m_ext'); (4) name of the companion; (5) spectroscopic redshift of the companion; (6) *K*-band absolute magnitude of the companion; (7) stellar mass ratio using the relation, $\log_{10} M_\star = 10.58 - 0.44\,(M_K + 23)$, to estimate stellar masses (Cappellari 2013); (8) angular distance on the sky between the main and companion galaxies; (9) projected distance in kpc using the redshift of the main galaxy.

Name	z	M_K (mag)	Companion	$z_{\rm comp}$	$M_{K,\rm comp}$ (mag)	$M_\star/M_{\star,\rm comp}$	$\theta_{\rm proj}$ (arcsec)	$D_{\rm proj}$ (kpc)
NGC0383*	0.017005	–	NGC0382	0.017442	–	–	34.20	12.4
NGC0507	0.016458	−26.04	NGC0058	0.018433	−24.86	15	87.61	32.1
NGC0708*	0.015886	–	NGC0705	0.015057	–	–	66.37	21.6
NGC0741	0.018294	–	NGC0742	0.019910	–	–	47.57	19.0
NGC1129	0.017472	−26.23	VV 085	0.016568	−23.82	255	25.98	9.3
NGC2258*	0.013539	–	–	–	–	–	39.14	11.2
NGC2274	0.016785	−25.70	NGC2275	0.016435	−24.59	13	115.51	40.3
NGC2672	0.014487	–	NGC2673	0.012508	–	–	25.98	9.3
NGC2693*	0.016083	−25.68	NGC2694	0.016908	−22.94	557	55.70	19.3

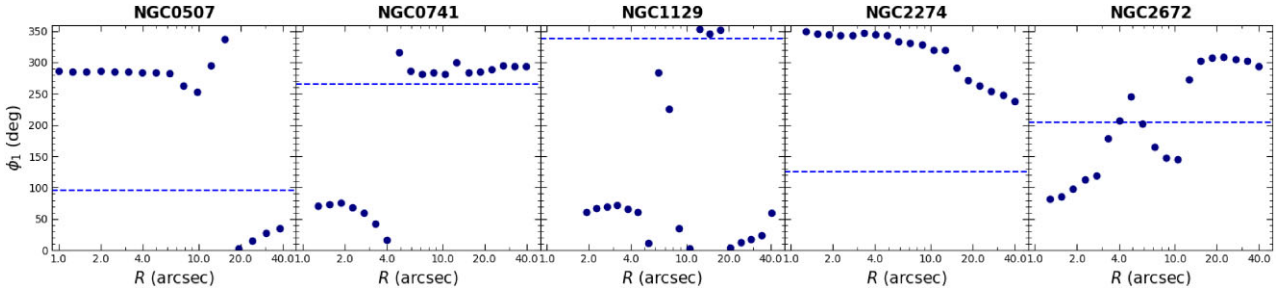

Figure 4. The position angle of the m_1 multipole as a function of radius for the five galaxies with the largest m_1 amplitudes. The dashed horizontal lines correspond to the position angle of the companion galaxy.

for both simulated galaxies, which is given by

$$I(r) = I_e \exp\left\{-b_n\left[\left(\frac{r}{r_e}\right)^{1/n} - 1\right]\right\}, \quad (4)$$

where r_e is the effective radius, I_e the intensity at the effective radius, n the Sérsic index, and b_n a constant parameter that only depends on n (Trujillo et al. 2004). The following choices were made in creating the simulated images:

(i) $r_{e,main} = 2.5\, r_{e,comp}$;
(ii) $F_{main} = 10\, F_{comp}$, where F represents the total flux;
(iii) $\theta_{proj} = 35$ (arcsec).

Finally, we added noise, n_i to each pixel from a normal distribution with zero mean and variance σ_i. The values of σ_i are proportional to the flux at each pixel, f_i, scaled by a constant factor that is chosen so that the total signal-to-noise ratio[3] of the mock is equivalent to that of the real data. Subsequently, we applied our ellipse fitting analysis to the main galaxy and found an m_1 amplitude profile $\lesssim$0.5 per cent at the radius of the companion, θ_{proj}. This test confirms that the physical origin of $m = 1$ perturbations is galaxy interactions (recent or ongoing).

In Fig. 4, we show the m_1 position angle, ϕ_1, profiles for all galaxies with high m_1 amplitudes. We find sharp transitions between the inner and outer regions, suggesting that physical processes (e.g. mergers, tidal interactions), occurring at different epochs, are shaping the profiles of ETGs. The m_1 position angle in the outer parts are often offset relative to the direction of the companion galaxy. This is perhaps not surprising when considering the relative time-scales of stellar orbits and the motion of the companion.

5.2 Strong gravitational lensing

In galaxy scale strong gravitational lensing studies, the most common type of profile assumed is an elliptical power-law model (EPL; Tessore & Metcalf 2015). Recently, a few studies have shown that assuming an EPL model for the mass distribution of the lens might not be enough to fit the data (e.g. Ballard et al. 2024; Nightingale et al. 2024; Stacey et al. 2024); this becomes increasingly the case with higher resolution data (e.g. Powell et al. 2022; He et al. 2023). As a result, attention has turned to the multipole model, particularly of order $m = 3, 4$, as a means for accounting for additional complexity (e.g. angular deviations) in the mass distribution.

[3]The total signal-to-noise ratio is computed as,

$$\mathrm{SNR} = \frac{\sum (f_i + n_i)}{\sqrt{\sum \sigma_i}}. \quad (5)$$

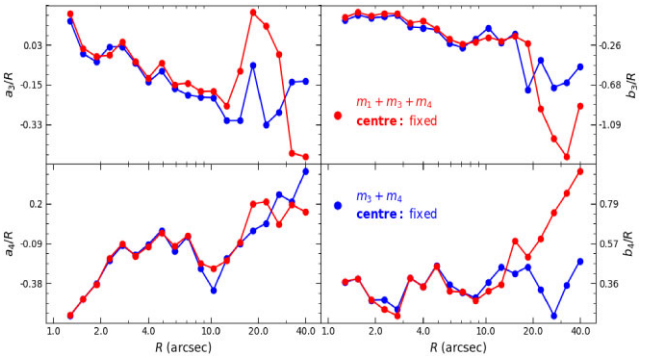

Figure 5. Radial profiles of the Fourier coefficients, a_m and b_m, of order $m = 3,\ 4$, for models 1 (blue) and 3 (red) measured for NGC2274. If the m_1 mode is not taken into account, the measurements of higher order multipoles are biased in the outer parts.

Models incorporating $m = 3,\ 4$ multipoles define isodensity contours with respect to a common centre, placing them in the model 1 category. However, as demonstrated in Section 4, this model fails to capture observed features such as lopsidedness in the outer parts of galaxies, where model 3 (which includes an $m = 1$ multipole) performs significantly better. Stacey et al. (2024) showed that $m = 3,\ 4$ multipoles in the mass distribution of three strongly lensed galaxies are favoured by the data (according to the Bayesian evidence). However, the multipole's Fourier coefficients (or amplitude and position angles) inferred from an isophotal analysis are not consistent with the strong lensing results. The isophotes in these galaxies display large radial offsets that are not captured in strong lens modelling. As an example, we show in Fig. 5 that the $m = 3,\ 4$ radial profiles of the Fourier coefficients differ in NGC2274 for model 1 and 3, which would correspond to strong lensing and isophotal analyses, respectively. This missing complexity in the mass distribution might explain the differences seen in Stacey et al. (2024).

An important consequence of ignoring the m_1 multipole complexity in mass models was recently explored by O'Riordan & Vegetti (2024). These authors simulate strong lenses using a model that includes an $m = 1$ perturbation, then fit the simulated data using a model that does not include m_1 but instead includes a dark matter subhalo, parametrized by a Navarro–Frenk–White profile (Navarro, Frenk & White 1996, 1997). The motivation behind this analysis was to quantify the rate of 'false-positive' detections of dark matter subhaloes that can occur if the mass model for the lensing galaxy

lacks complexity. Their findings suggest that the probability of false positives for lenses with ∼10 per cent m_1 amplitudes is almost an order of magnitude higher than for models with ∼1 per cent m_4 amplitudes (which are the typical values). It is therefore important that both these types of complexity be considered when modelling the lensing galaxy.

For galaxies with high m_1 amplitudes, the profiles typically peak around ∼6−10 kpc. For a galaxy-scale lens at $z = 0.2/0.8$, an Einstein radius of $r_E \sim 1$ arcsec corresponds to $r_E \sim 3.4/7.7$ kpc in physical units. Given that strong lensing is particularly sensitive to the mass distribution near the Einstein radius, m_1 amplitudes of up to ∼10 per cent are to be expected when modelling strong lenses.

5.3 Galactic dynamics

The presence of an $m = 1$ multipole in real galaxies could also affect dynamical models. This is true for both the technical aspects of generating the model, as well as the physical interpretation of the dynamics. Many dynamical models are restricted to axisymmetry (e.g. Jeans anisotropic models; Cappellari 2008) in the mass distribution, which implies a common centre for all mass components, no isophotal twists and certainly no $m = 1$ multipole (asymmetry). At the most massive end, real galaxies often exhibit isophotal twists, as well as misalignments between kinematic and photometric position angles, which are both evidence for triaxiality. Triaxial implementations of dynamical models (e.g. Pilawa et al. 2022; Quenneville, Liepold & Ma 2022) are able to account for such features. Even so, twists and misalignments are point-symmetric perturbations, meaning there is symmetry about the origin. Real asymmetry in the mass distribution resulting in a strong $m = 1$ multipole implies that the galaxy is out of dynamical equilibrium, since such a configuration is not stable under self-gravity. Unlike gravitational lensing, dynamical equilibrium is a fundamental assumption of any dynamical model and thus large $m = 1$ multipoles pose conceptual challenges to modelling the dynamics of such galaxies.

Modern observations of stellar kinematics (e.g. the MASSIVE sample) routinely reach the physical scales which here are found to exhibit large $m = 1$ modes. However, dynamical modelling of massive ETGs out to ∼10 kpc has yet to be conducted systematically. One example was presented in Pilawa et al. (2022), where Integral Field Unit (IFU) data for NGC 2693 was modelled by a triaxial orbit-superposition code. Interestingly, isophotal twists are measured and attributed to the impact of a companion galaxy. The magnitude of this effect on measurements of the dynamical mass and internal structure in the presence of $m = 1$ multipoles remains to be quantified. Given that they are most prevalent in the outermost luminous regions where the stellar density is low, it is likely that the impact on existing dynamical models is minimal. This is true for the vast majority of dynamical studies, which make measurements at or within the effective radius, $R_e \sim 10$ kpc. Conversely, dynamical constraints on dark matter would arise mostly from these outer low-stellar density regions, and so those measurements might be more affected by unaccounted for asymmetries.

6 CONCLUSIONS

We have measured perturbations to the isophotes of ETGs in the local Universe, selected from the MASSIVE survey. A novel aspect of our analysis is the use of the $m = 1$ multipole instead of allowing the centre of the elliptical isophotes to vary with distance from the galactic centre, as is common practice in ellipse fitting analyses (e.g. Hao et al. 2006; Goullaud et al. 2018). This parametrization enables the model to capture features such as lopsidedness/skewness, which are often not included in mass models used in strong gravitational lensing and galactic dynamics studies. While such asymmetries may not be significant in the majority of ETGs, they do become relevant for specific cases, such as galaxies that have recently undergone an interaction.

A practical approach to determine if an $m = 1$ multipole should be included in the mass model is to first identify close companions on the sky and determine whether they are physically associated with the main galaxy (i.e. the lensing galaxy, in the case of strong lensing). This requires spectroscopic redshift measurements for both the main and companion galaxies. Without redshift information, it may not be appropriate to assume that an $m = 1$ multipole is unnecessary. This challenge is further exacerbated at higher redshifts, where companion galaxies can become to faint to detect.

We found that the amplitude of the m_1 multipole can reach values as high as 10 per cent on scales relevant to strong lensing, but only in galaxies that are undergoing interactions with other galaxies. We argue that models aiming to describe the mass distribution of ETGs should incorporate this level of complexity. Failure to account for it can lead, for instance, to false-positive detections of dark matter subhaloes in strong lensing studies (e.g. O'Riordan & Vegetti 2024) or to an inability for the model to focus light rays on the source plane accurately (Nightingale et al. in preparation). In two upcoming works, Lange et al. (in preparation) and Amvrosiadis et al. (in preparation), we will fit mass models incorporating an $m = 1$ order multipole perturbation to the distribution of mass in two strongly lensed dusty star-forming galaxies.

SOFTWARE CITATIONS

This work uses the following software packages: NUMPY, MATPLOTLIB, ASTROPY, SCIPY, APLPY.

ACKNOWLEDGEMENTS

AA, QH, CSF, and SC are supported by ERC Advanced Investigator grant, DMIDAS [GA 786910] to CSF. We acknowledge support from STFC consolidated grant ST/X001075/1. This work used the DiRAC@Durham facility managed by the Institute for Computational Cosmology on behalf of the STFC DiRAC HPC Facility (www.dirac.ac.uk). The equipment was funded by BEIS capital funding via STFC capital grants ST/K00042X/1, ST/P002293/1, ST/R002371/1, and ST/S002502/1, Durham University and STFC operations grant ST/R000832/1. DiRAC is part of the UK National e-Infrastructure.

DATA AVAILABILITY

All data used in this work are publicly available.

REFERENCES

Ballard D. J., Enzi W. J. R., Collett T. E., Turner H. C., Smith R. J., 2024, MNRAS, 528, 7564
Bender R., Moellenhoff C., 1987, A&A, 177, 71
Bender R., Doebereiner S., Moellenhoff C., 1988, A&AS, 74, 385
Bender R., Surma P., Doebereiner S., Moellenhoff C., Madejsky R., 1989, A&A, 217, 35
Blumenthal G. R., Faber S. M., Primack J. R., Rees M. J., 1984, Nature, 311, 517

Cappellari M., 2002, MNRAS, 333, 400
Cappellari M., 2008, MNRAS, 390, 71
Cappellari Michele, 2013. The Astrophysical Journal, 778, L2
Chaware L., Cannon R., Kembhavi A. K., Mahabal A., Pandey S. K., 2014, ApJ, 787, 102
Cohen Jacob S, Fassnacht Christopher D, Oâ€™Riordan Conor M, Vegetti Simona, 2024. Monthly Notices of the Royal Astronomical Society, 531, 3431
Foreman-Mackey D., Hogg D. W., Lang D., Goodman J., 2013, PASP, 125, 306
Frenk C. S., White S. D. M., Efstathiou G., Davis M., 1985, Nature, 317, 595
Goullaud C. F., Jensen J. B., Blakeslee J. P., Ma C.-P., Greene J. E., Thomas J., 2018, ApJ, 856, 11
Hao C. N., Mao S., Deng Z. G., Xia X. Y., Wu H., 2006, MNRAS, 370, 1339
He Q. et al., 2023, MNRAS, 518, 220
Hezaveh Y. D. et al., 2016, ApJ, 823, 37
Lange Samuel C, Amvrosiadis Aristeidis, Nightingale James W, He Qiuhan, Frenk Carlos S, Robertson Andrew, Cole Shaun, Massey Richard, Cao Xiaoyue, Li Ran, Wang Kaihao, 2025. Monthly Notices of the Royal Astronomical Society, 539, 704
Ma C.-P., Greene J. E., McConnell N., Janish R., Blakeslee J. P., Thomas J., Murphy J. D., 2014, ApJ, 795, 158
Navarro J. F., Frenk C. S., White S. D. M., 1996, ApJ, 462, 563
Navarro J. F., Frenk C. S., White S. D. M., 1997, ApJ, 490, 493
Nightingale J. W., Massey R. J., Harvey D. R., Cooper A. P., Etherington A., Tam S. I., Hayes R. G., 2019, MNRAS, 489, 2049
Nightingale J. W. et al., 2023, MNRAS, 521, 3298
Nightingale James W, He Qiuhan, Cao Xiaoyue, Amvrosiadis Aristeidis, Etherington Amy, Frenk Carlos S, Hayes Richard G, Robertson Andrew, Cole Shaun, Lange Samuel, Li Ran, Massey Richard, 2024. Monthly Notices of the Royal Astronomical Society, 527, 10480
O'Riordan C. M., Vegetti S., 2024, MNRAS, 528, 1757
Pasquali A. et al., 2006, ApJ, 636, 115
Pilawa J. D., Liepold C. M., Delgado Andrade S. C., Walsh J. L., Ma C.-P., Quenneville M. E., Greene J. E., Blakeslee J. P., 2022, ApJ, 928, 178
Planck Collaboration XIII, 2016, A&A, 594, A13
Powell D. M., Vegetti S., McKean J. P., Spingola C., Stacey H. R., Fassnacht C. D., 2022, MNRAS, 516, 1808
Quenneville M. E., Liepold C. M., Ma C.-P., 2022, ApJ, 926, 30
Sérsic J. L., 1963, Bol. Asociación Argentina Astron., 6, 41
Stacey H. R., Powell D. M., Vegetti S., McKean J. P., Fassnacht C. D., Wen D., Oâ€™Riordan C. M., 2024. Astronomy & Astrophysics, 688, A110
Tessore N., Metcalf R. B., 2015, A&A, 580, A79
Trujillo I., Erwin P., Asensio Ramos A., Graham A. W., 2004, AJ, 127, 1917
Van de Vyvere L., Gomer M. R., Sluse D., Xu D., Birrer S., Galan A., Vernardos G., 2022, A&A, 659, A127

APPENDIX A: HIGHER ORDER MULTIPOLE PROFILES

In Fig. A1, we show the radial profiles for the m_3 and m_4 multipoles. The maximum amplitudes of these higher order multipoles are consistent with previous studies (∼2 per cent; Goullaud et al. 2018). In both panels, we coloured in blue, galaxies that display elevated m_1 amplitudes (same as in Fig. 3). An interesting trend is that galaxies with high m_1 amplitudes also tend to exhibit the highest

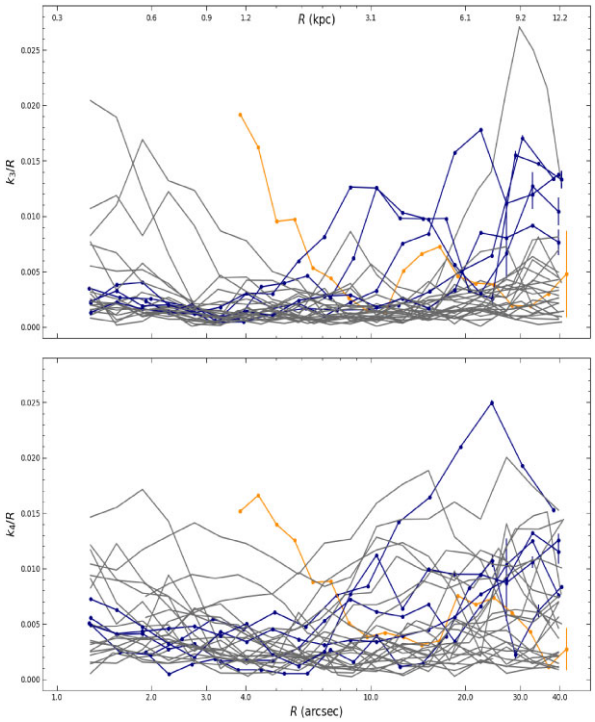

Figure A1. Same as Fig. 3 but for the $m = 3,\ 4$ multipoles. We coloured in blue all galaxies with maximum $m = 1$ amplitude above 2 per cent (bottom row cutouts in Fig. 3).

m_3 amplitudes at $R \gtrsim 3$ kpc.[4] This correlation, however, does not hold for the m_4 multipole.

This trend suggests that both $m = 1$ and $m = 3$ order multipole perturbations are short-lived and quickly dissipate, explaining the high amplitudes observed in galaxies with recent or ongoing interactions. In contrast, $m = 4$ order perturbations (e.g. bars in galaxies) are more stable and are therefore observed in more galaxies, regardless of recent or ongoing interactions with companions.

[4]The galaxy with the highest maximum m_3 amplitude, NGC0383, has low m_1 amplitude. However, this galaxy also has a companion (see top panel in Fig. 3).

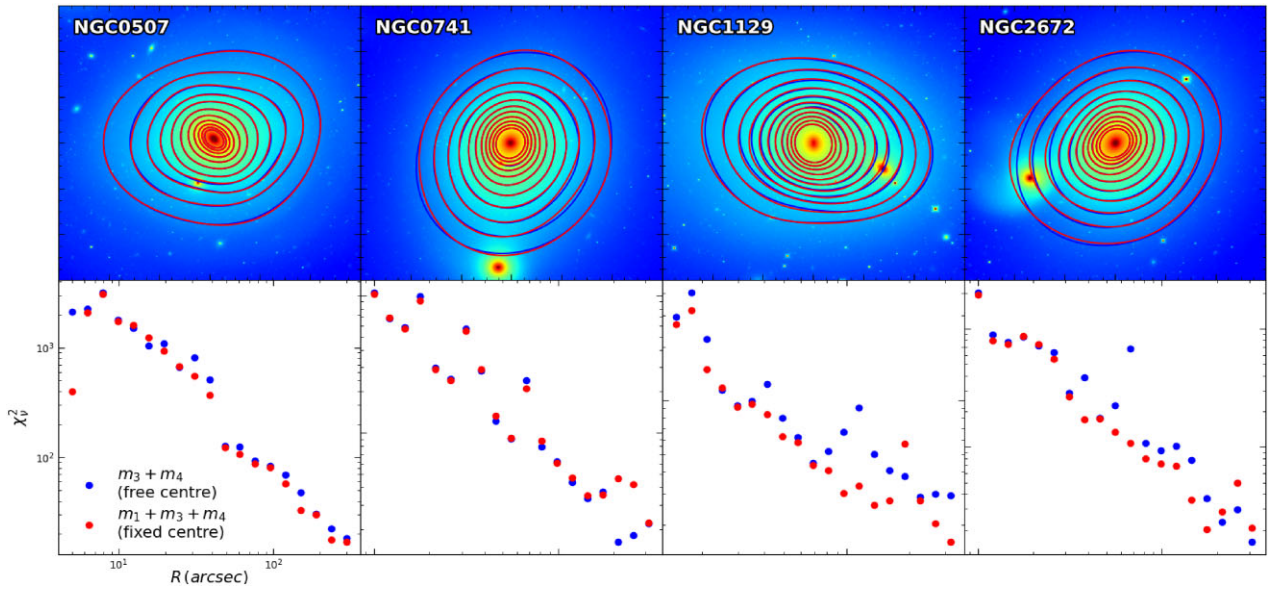

Figure A2. The reduced chi-square of isophotes using models 2 and 3 (see Section 4), in blue and red, respectively, for galaxies with high $m = 1$ amplitudes. The two models appear to fit the data equally well for all radii, with model 3 performing marginally better.

This paper has been typeset from a TEX/LATEX file prepared by the author.